GEOLOGY

Pure climb creep mechanism drives flow in Earth's lower mantle

Francesca Boioli,[1]* Philippe Carrez,[1] Patrick Cordier,[1†] Benoit Devincre,[2] Karine Gouriet,[1] Pierre Hirel,[1] Antoine Kraych,[1] Sebastian Ritterbex[1‡]

At high pressure prevailing in the lower mantle, lattice friction opposed to dislocation glide becomes very high, as reported in recent experimental and theoretical studies. We examine the consequences of this high resistance to plastic shear exhibited by ringwoodite and bridgmanite on creep mechanisms under mantle conditions. To evaluate the consequences of this effect, we model dislocation creep by dislocation dynamics. The calculation yields to an original dominant creep behavior for lower mantle silicates where strain is produced by dislocation climb, which is very different from what can be activated under high stresses under laboratory conditions. This mechanism, named pure climb creep, is grain-size–insensitive and produces no crystal preferred orientation. In comparison to the previous considered diffusion creep mechanism, it is also a more efficient strain-producing mechanism for grain sizes larger than ca. 0.1 mm. The specificities of pure climb creep well match the seismic anisotropy observed of Earth's lower mantle.

INTRODUCTION

Earth dissipates its internal heat through large-scale mantle convection. Although made of crystalline rocks, the mantle can flow like a viscous fluid at geological time scale. This behavior is governed by creep mechanisms, which involve the motion of crystal defects at the microscopic scale. The nature of the defects and the creep mechanisms involved have profound implications on the rheology and hence, on the dynamics of our planet. Recent progress in high-pressure experiments has expanded our capability to perform deformation experiments at high pressure and at high temperature. Recently, a few studies have shown that ringwoodite and bridgmanite can be deformed experimentally provided that extremely high stresses (of the order of the GPa) are applied (*1*–*3*). However, these data were acquired at laboratory strain rates (of the order of 10^{-5} s^{-1}) because reproducing creep deformation at high *P*,*T* at the extremely slow strain rates of the mantle (of the order of 10^{-14} s^{-1}) is still out of reach. Here, we report results from numerical simulations of creep, which reveal the importance of a mechanism where dislocations are sources and sinks for vacancy diffusion and produce plastic shear by climb. By introducing a characteristic distance for diffusion smaller than the grain size, this pure climb creep mechanism is found to be more efficient than the standard Nabarro-Herring (NH) (or Coble) creep features. Pure climb creep, which is grain size–independent, is then a very efficient mechanism that accounts for the mantle flow in planetary interiors, even under very high temperatures and high pressures, and does not produce crystallographic preferred orientation.

To describe plastic flow in crystalline rocks, one commonly considers two distinct potential processes classified as diffusion creep and dislocation creep (Fig. 1). In diffusion creep, plastic strain results directly from the motion of crystal point defects. Vacancy concentration close to a grain boundary under tension, being greater than that close to a grain boundary under compression, leads to a net flux of matter between sources and sinks (Fig. 1A). At high temperatures, vacancies can diffuse through the bulk of the grain as considered in the NH creep mechanism (*4*, *5*) or along the grain boundaries as proposed by Coble (*6*). The grain size defines the characteristic distance between sources and sinks and strongly limits the efficiency of both mechanisms with potential implications on the convection of terrestrial planets (*7*, *8*). Dislocation creep (Fig. 1B), as commonly observed in metallurgy, takes part in crystal recovery processes associated with heat treatments (*9*–*11*). Plastic strain is produced by the glide of a fraction of dislocations that are made free to move owing to two thermally activated mechanisms (*12*), that is, cross-slip (screw dislocations deviating from their initial glide plane) and climb (motion out of the glide planes of nonscrew dislocations after absorbing point defects) (*13*). Contrary to diffusion creep (NH or Coble), dislocation creep can produce crystal preferred orientations potentially strong enough to yield seismic anisotropy (*14*). Characterized by a higher stress sensitivity, dislocation creep is most importantly grain size–insensitive. For this reason, the average grain size is considered the key parameter in determining whether diffusion creep or dislocation creep controls crystal plasticity in the deep Earth. Unfortunately, rocks' grain size is not known in Earth's lower mantle. Here, we show that new developments in dislocation dynamics (DD) and creep modeling in high-pressure minerals shed new light on dislocation creep mechanisms and their relevance in mantle conditions.

RESULTS AND DISCUSSION

First, using DD simulation (*12*, *15*), we investigated the complex interplay between dislocation glide and dislocation climb. These simulations are instructive in understanding how, during creep processes, the glide mobility of dislocations competes with their climb mobility. Figure 2 shows the ratio (v_g/v_c) of the glide over the climb velocity as a function of the temperature and the applied stress. Both mobilities strongly depend on the crystal structure and on specific atomic configurations that build the dislocation cores. The climb velocity also depends on the diffusivity of point defects. In olivine, which controls the rheology of upper mantle rocks, glide is always much faster than climb (see Fig. 2A), leading to a creep behavior very close to the one originally proposed by Weertman [see the study of Boioli *et al.* (*12*) and Keralvarma *et al.* (*16*)]. However, it has been already emphasized that the contribution of climb to high-temperature creep of olivine cannot be ignored (*17*). For the high-pressure phases existing in the deeper mantle (wadsleyite, ringwoodite, and bridgmanite), experiments available so far do not provide information on dislocation mobility. However, recent modeling based on atomic-scale computations has successfully yielded dislocation glide velocity (v_g)

[1]Unité Matériaux et Transformations, UMR CNRS 8207, Université Lille 1, Villeneuve d'Ascq, France. [2]Laboratoire d'Etude des Microstructures, CNRS-ONERA, Chatillon, France.
*Present address: Institut Lumière Matière, Universitè Lyon 1, Villeurbanne, France.
†Corresponding author. Email: patrick.cordier@univ-lille1.fr
‡Present address: Geodynamics Research Center, Ehime University, 2-5 Bunkyocho, Matsuyama 790-8577, Japan.

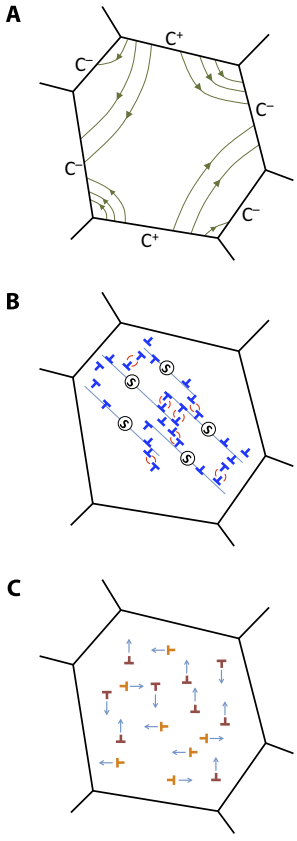

Fig. 1. Creep models. (**A**) Diffusion creep where grain boundaries act as sources (C^+) and sinks (C^-) for vacancies. The schematic represented here corresponds to NH creep where vacancies diffuse through the lattice. In Coble, creep vacancies would diffuse along grain boundaries. (**B**) Dislocation creep. The Weertman model where gliding dislocations are emitted by sources (S). Interactions are then released by some recovery mechanisms (red arrows) such as climb. (**C**) Pure climb creep. Strain is produced by climb motion of two orthogonal slip systems, which exchange vacancies.

models for wadsleyite (*18*), ringwoodite (*19*), and bridgmanite (*20*), which are able to reproduce the rare experimental data available well. This shows that the high stress levels observed experimentally (*1*–*3*) result from the very high lattice friction exhibited by wadsleyite, ringwoodite, and bridgmanite at high pressure. Besides particularities of each crystal structure and of its defects, this general trend reflects the strong influence of pressure on bond strengths, especially the ionocovalent Si-O bond (a fact that is already noticeable in the pressure dependence of elastic constants). It is only at high stresses (see Fig. 2, B and C) that dislocation glide can be activated to produce strain and that standard dislocation creep is expected. However, at lower stresses (which one could expect in the convecting mantle), the situation is drastically different. Below ca. 1.2 GPa for ringwoodite (Fig. 2B) and ca. 1.8 GPa for bridgmanite (Fig. 2C), the dislocation glide velocity is much slower than climb velocity. Hence, the efficiency of dislocation glide as a strain-producing mechanism becomes negligible compared to climb. To the best of our knowledge, there is only one case in materials science where this situation is faced: quasicrystals. Quasicrystals are model metallic alloys with atomic arrangements that induce symmetries that are long assumed to be forbidden in periodic crystals. In quasicrystals, the dense planes are very corrugated, making shear along these planes necessarily difficult. Thus, lattice friction is very high and plastic shear can only be achieved at high temperatures by edge dislocations moving by pure climb (*21*–*23*).

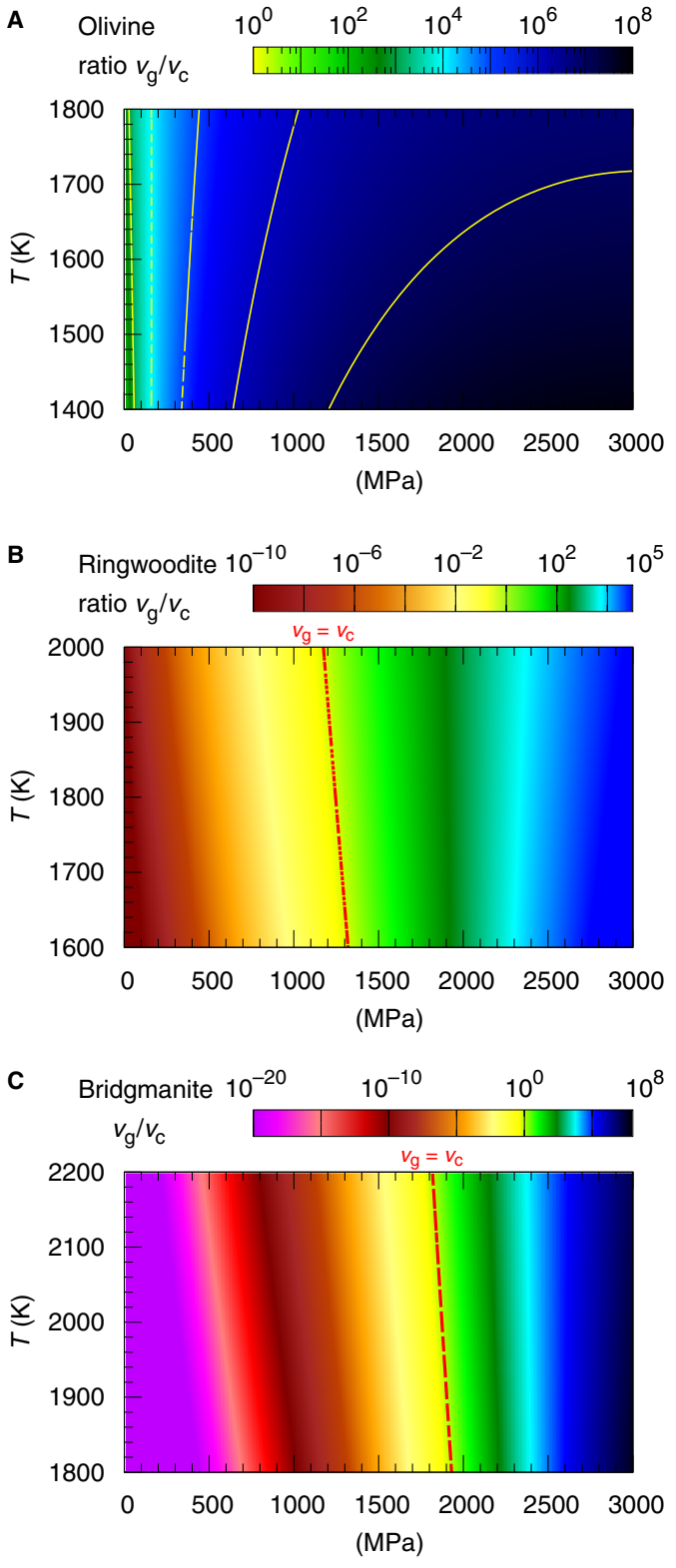

Fig. 2. Comparison between the glide velocity (v_g) and the climb velocity (v_c) of dislocations. The ratio of v_g/v_c is mapped as a function of temperature and resolved stress for (**A**) olivine at ambient pressure, (**B**) ringwoodite at 20 GPa, (**C**) and bridgmanite at 30 GPa. The red line where $v_g = v_c$ indicates the transition between two regimes. At high stress (green to blue), glide is the strain-producing mechanism. At low stress (yellow to purple), climb dominates.

The outcome that climb could be a large strain-producing mechanism (and not only a recovery process) has long been predicted theoretically (*24*). It has also been established experimentally in materials where dislocation glide can be hindered geometrically, that is, for instance, in some hexagonal single crystals compressed perpendicular to the basal plane: Mg (*25*, *26*) and Be (*27*).

High lattice friction in high-pressure phases leads to reconsideration of the processes operating during dislocation creep because climb becomes the dominant strain-producing mechanism. The next question then is whether pure climb is also a dominant creep mechanism for high-pressure silicates under mantle conditions. To address this new question and evaluate the potential contribution of climb to mantle rheology, we calculate pure climb creep rates for bridgmanite and compare them with diffusion creep rates. To do that, the two-dimensional (2D) DD model previously used to investigate creep in olivine is modified here to consider only pure climb. Two orthogonal slip systems, [100](010) and [010](100), are introduced in the simulation. Dislocations are parallel straight lines of pure edge characters, perpendicular to the reference 2D plane of the simulation. Their Burgers vector lies in the reference plane and defines the slip direction. The climb direction is in the reference plane and is orthogonal to both the Burgers vector and the line direction. The force acting on each dislocation depends on the stress fields at the dislocation positions, which results from the action of both the external loading applied on the simulation cell and from the stress fields of all other dislocations. It is given by the so-called Peach-Koehler equation (see detailed description in Materials and Methods). In pure climb creep (*24*), vacancies migrate from edge dislocations with their Burgers vectors roughly parallel to the tensile axis (case 1 in Fig. 3A) to edge dislocations with their Burgers vectors roughly perpendicular to the tensile axis (case 2 in Fig. 3A). This vacancy exchange allows dislocations to move with a climb velocity, which not only depends on the mechanical force acting on the dislocation but also on the "chemical force" arising from the gradient in the vacancy concentration and produce plastic strain. At the steady state, dislocation multiplication is counterbalanced by dislocation density reduction due to annihilation events, that is, the destruction of pairs of dislocations with opposite Burgers vectors coming across each other. We find that the steady state is reached, characterized by an average linear increase of the plastic strain with time, as shown in Fig. 3B and a constant dislocation density. An example of the resulting dislocation microstructure is shown in Fig. 3 (C and D). When comparing the steady-state strain rates obtained from pure climb DD models with diffusion creep rates (Fig. 4), dislocation climb is always a more efficient plastic deformation mechanism (provided that grain size is in excess of 0.1 mm) than diffusion creep under lower mantle conditions.

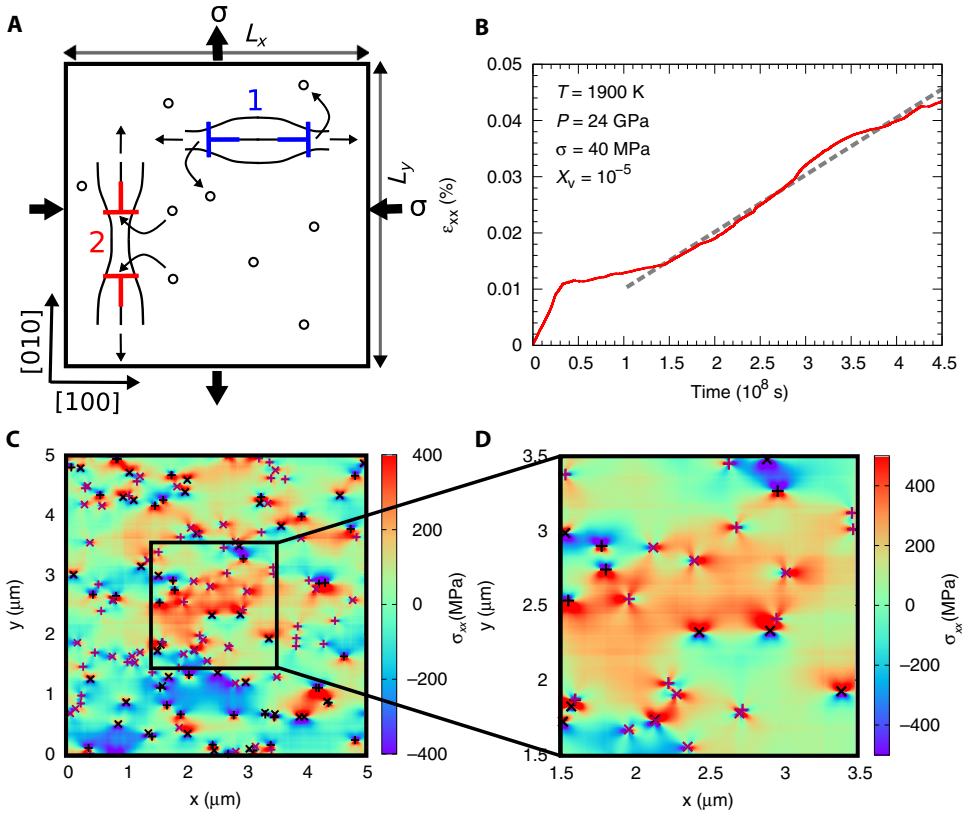

Fig. 3. Pure climb creep simulation in bridgmanite. (**A**) Sketch of the 2D simulation box and of the loading condition. The chosen loading conditions were set in analogy with the conditions usually used for describing NH creep. They correspond to a pure shear loading. Two slip systems are considered. Here, dislocations characterized by [010] Burgers vector (labeled as "1" and shown in blue) move in response to the tensile stress along the [100] climb direction by emitting vacancies. The excess of vacancies created by these dislocations is absorbed by the dislocations with [100] Burgers vector (slip system as "2" and shown in red), which move in response to the compressive stress along the [100] direction by absorbing vacancies. (**B**) DD stress-strain curve obtained by applying a creep stress σ of 40 MPa at $T = 1900$ K and $P = 24$ GPa. In this particular case, the initial dislocation density is 10^{12} m^{-2}, and an equilibrium vacancy concentration of $X_v = 10^{-5}$ is assumed. After an initial transient stage where dislocation multiplication occurs, the steady state is attained and the steady-state strain rate value is extracted (dashed line slope). (**C**) Dislocation microstructure and σ_{xx} stress field extracted from the creep simulation at $\varepsilon_{xx} = 0.045\%$. (**D**) Detail of the dislocation microstructure shown in (C). Black (purple) symbols indicate the dislocations with [100] ([010]) Burgers vector, whereas plus (cross) symbols are used to denote the positive (negative) sign of their Burgers vector.

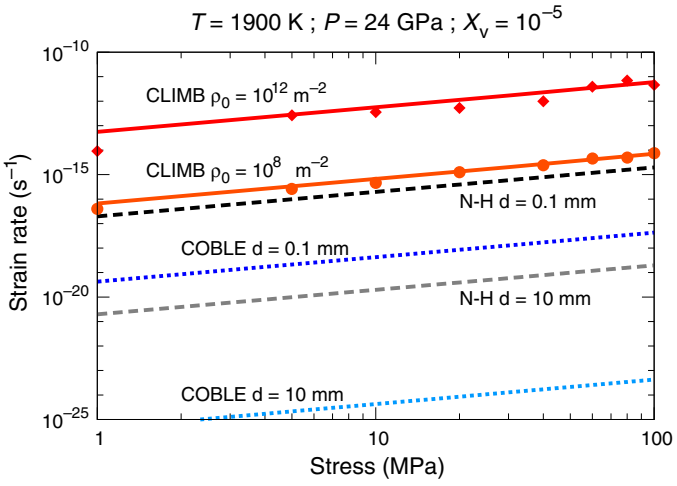

Fig. 4. Comparison between the strain rates obtained by pure climb creep and by diffusion creep. Strain rate values resulting from diffusion creep are calculated (see Supplementary Materials) for the Coble (blue dotted lines) and the NH ("N-H," black and gray dashed lines) for two grain sizes: 0.10 and 10 mm. They are compared to strain rates resulting from pure climb creep (red symbols) calculated as shown in Fig. 3 for dislocation densities (ρ_o) ranging from 10^8 to 10^{12} m^{-2}. For grain sizes larger than ca. 0.1 mm, pure climb creep is a more efficient strain-producing mechanism than diffusion creep.

CONCLUSION

Here, we show that in bridgmanite, creep dominated by dislocation pure climb is a viable mechanism that is able to promote plastic flow at rates compatible with those expected in the mantle. Pure climb creep involves vacancy diffusion as NH creep does; however, the characteristic diffusion length (between vacancy sources and sinks) is controlled by the dislocation density instead of the grain size. The former being necessarily smaller than the latter, pure climb creep becomes more efficient than NH creep when grains are larger than 0.1 mm. One of the major implications of this study is to show that grain size, which is a major unknown in the mantle, is not a controlling parameter of the mantle viscosity as assumed for many years. Moreover, climb involves no lattice rotation. Hence, although strain is produced by dislocation motion, pure climb creep does not produce crystal preferred orientation. Thus, our model is compatible with the absence of strong seismic anisotropy in Earth's lower mantle.

MATERIALS AND METHODS

Glide and climb velocity v_g and v_c

Silicates under high pressure are characterized by high lattice friction. To move, a dislocation must overcome the intrinsic resistance of the lattice (which is also related to the specific atomic arrangements that build the dislocation core). This is quantified by the Peierls potential V_P. The derivative of V_P defines the Peierls stress τ_P, which is commonly viewed as the critical resolved shear stress at 0 K, and as such, gives the mechanical measure of the lattice friction experienced by dislocations. At finite temperature, dislocation motion over the Peierls potential is assisted by the conjugate effect of stress and thermal activation. During this process, the dislocation does not move as a straight line but through the nucleation and propagation of kink pairs. The kink-pair nucleation process corresponds to a small segment of the dislocation line that bulges over the Peierls potential. The further propagation along the dislocation line of the kinks is responsible for the glide of the whole dislocation into the next stable position in the crystal lattice. The kink-pair nucleation process is usually associated with a critical change in enthalpy that has to be supplied by thermal activation under a given stress. Following the kink-pair mechanism, the resulting glide velocity of a dislocation undergoing a uniform resolved shear stress τ^* is described with the following formulation (Eq. 1)

$$v_g = v_0 \exp\left[-\frac{\Delta H_0(1-(\tau^*/\tau_P)^p)^q}{k_B T}\right] \quad (1)$$

where k_B is the Boltzmann constant and T is the temperature. ΔH_0, parameters p and q, and pre-exponential term v_0 are dislocation intrinsic quantities describing the glide velocities according to a kink-pair mechanism of the dislocation. The theoretical description of dislocation motion involving the kink-pair mechanism has been recently successfully applied to the understanding of elementary deformation processes in ringwoodite (*19*) and bridgmanite (*20*). Glide velocities for the easiest slip systems, that is $\frac{1}{2}$<110>{110} dislocations in ringwoodite and [100](010) in bridgmanite, were thus computed in this study using the set of parameters listed in table S1. It should be recalled here that all these parameters come from atomistic calculations based on either first-principles calculations (ringwoodite) or empirical potential parameterizations (bridgmanite). In the case of bridgmanite, the relevance of the empirical parameterization to large (nonelastic) displacements was further validated with a comparison to ab initio calculations of the so-called generalized stacking fault energies at each pressure of interest in the present study. Moreover, as shown by Ritterbex *et al.* (*19*) or Kraych *et al.* (*20*), it should be pointed out that atomistic calculations led to glide velocities for dislocations, which correspond to resolved shear stresses that agree with flow stresses extracted from recent experimental measurements. In olivine, the parameters associated with the glide mobility were obtained by fitting experimental data at ambient pressure from various sources [see for instance the work of Durinck *et al.* (*28*) and references therein]. In table S1, we report the parameters used to describe the velocity of [100] dislocations, which have been found to govern the plastic behavior at high temperatures ($T > 1300$ K).

With the usual assumption that climb is controlled by vacancy diffusion and that the dislocation line is saturated with jogs (steps along the dislocation line that act as sinks/sources of vacancies), the climb velocity under steady-state conditions is given by the following analytical expression (*29*)

$$v_c = \eta \frac{D^{sd}}{b}\left[\exp\left(\frac{\tau_c^* \Omega}{k_B T}\right) - \frac{X_\infty}{X_v}\right] \quad (2)$$

where D^{sd} is the self-diffusion coefficient, Ω is the vacancy formation volume, and η is a geometrical factor that depends on the geometry of the flux field. X_∞ is the vacancy concentration far from the dislocation, whereas X_v is the equilibrium vacancy concentration in a bulk at a given temperature T.

According to Eq. 2, climb velocities (as plotted in Fig. 2) were computed for the three minerals as a function of τ_c^*, the effective climb stress, at the equilibrium bulk vacancy concentration ($X_v = X_\infty$). Relevant parameters corresponding to vacancy self-diffusion coefficient

are given in table S2. To explicitly introduce the dependence of the diffusion coefficient on the vacancy concentration, it is useful to rewrite it as follows

$$D^{sd} = X_v D^v = X_v v_a \ell^2 \exp\left(-\frac{\Delta H^m}{k_B T}\right) = D^{sd,0} \exp\left(-\frac{\Delta H^m}{k_B T}\right) \quad (3)$$

where D^v is the vacancy diffusion coefficient, given by the product of the attempt jump frequency, the square of the jump distance, and the jump probability. The latter is given by the exponential term $\exp\left(-\frac{\Delta H^m}{k_B T}\right)$, where the barrier height ΔH^m is the vacancy migration enthalpy. From diffusion experiments, it is usually possible to extract two distinct parameters: the exponential prefactor of the self-diffusion coefficient $D^{sd,0}$ and the vacancy migration enthalpy ΔH^m. The climb velocities plotted in Fig. 2 were obtained by inserting the experimental values of $D^{sd,0}$ and ΔH^m for the slowest diffusing species in Eq. 3 for the three minerals from different sources in the literature. The vacancy formation volume was calculated from the unit cell volume.

Climb creep modeling using 2.5D DD

2D DD simulations were performed to model creep produced by climb in $MgSiO_3$ bridgmanite. Two orthogonal slip systems, [100](010) and [010](100), were considered. The Burgers vector amplitude b was set to the value of the [100] lattice parameter (b = 4.65 Å). Within this model, the dislocations were materialized as parallel straight lines of pure edge characters, perpendicular to the reference 2D plane of the simulation. Their Burgers vector $\boldsymbol{b}$ lies in the reference plane and defines the slip direction. The climb direction $\boldsymbol{n}$ is then identified by the direction in the reference plane orthogonal to both the Burgers vector and the line direction $\boldsymbol{l}$ ($\boldsymbol{n} = \boldsymbol{l} \times \boldsymbol{b}$). The positive orientation of $\boldsymbol{n}$ is taken along the vacancy emission direction, that is, from the dislocation core, the direction pointing to the extra half-plane that characterizes an edge dislocation. By analogy with NH loading conditions (*4*, *5*), a constant loading was applied with a tensile stress along the [010] direction and a compressive stress along the [100] direction. Under these conditions, maximum resolved stresses on climb planes were ensured with [010] dislocations climbing by emitting vacancies, while [100] dislocations climb by absorbing them (see Fig. 3A). As a result, the average vacancy concentration in the bulk remained constant because the excess of vacancies created by one slip system was absorbed by the other slip system. The initial vacancy concentration X_v was assumed to be homogeneous. Initial dislocation microstructures were built for different values of dislocation density (from 10^8 to 10^{13} m^{-2}) by varying the size L of the simulation box from 3 to 1000 μm, keeping the initial dislocation number equal to 100. The simulation area corresponds therefore to a square of size L on which periodic boundary conditions were applied in the reference plane.

Once an initial random microstructure was set, the five following steps were iteratively repeated during the course of the simulation.

Force calculations.

The force acting on each dislocation i depends on the stress fields at the dislocation position x_i and it is given by the so-called Peach-Koehler equation

$$\boldsymbol{F}_i^{PK} = \mathbf{b}_i \cdot \left(\boldsymbol{\sigma}_{app}(x_i) + \boldsymbol{\sigma}_{int}(x_i)\right) \times \boldsymbol{l}_i \quad (4)$$

where $\boldsymbol{b}_i$ and $\boldsymbol{l}_i$ are the Burgers vector and line direction of the ith dislocation, respectively, $\boldsymbol{\sigma}_{app}$ is the external applied load, and $\boldsymbol{\sigma}_{int}$ is the internal stress field induced by the dislocation microstructure. The component of the force contributing to climb, along the climb direction $\boldsymbol{n}_i$, is then given by

$$\boldsymbol{F}_{c,i} = \boldsymbol{F}_i^{PK} \cdot \boldsymbol{n}_i = \left[\mathbf{b}_i \cdot \left(\boldsymbol{\sigma}_{app}(x_i) + \boldsymbol{\sigma}_{int}(x_i)\right) \times \boldsymbol{l}_i\right] \cdot \boldsymbol{n}_i \quad (5)$$

Velocity calculation and displacement predictions.

According to Eq. 2, the climb velocity (Eq. 6) of each dislocation i not only depends on the mechanical force acting on the dislocation itself but also on the chemical force arising from the gradient in the vacancy concentration. Here, the effective stress in the climb direction is equivalent to the component of the Peach-Koehler force contributing to climb $\boldsymbol{F}_{c,i}$ divided by the amplitude of the Burgers vector b

$$v_{c,i} = \frac{2\pi}{\ln\left(1/(2\sqrt{\rho}\, r_c)\right)} \frac{X_v D^v}{b} \left[\exp\left(\frac{F_{c,i}\, \Omega}{b\, k_B T}\right) - \frac{X_\infty}{X_v}\right] \quad (6)$$

Again, X_v is the equilibrium vacancy concentration and X_∞ is the vacancy concentration at a distance R from the dislocation, which we allowed to vary in time and space during the simulations. R is taken as the half of the average dislocation distance [$R = 1/(2\sqrt{\rho})$], where ρ is the instantaneous dislocation density and r_c is the core radius that we took equal to 5b.

To explicitly introduce the dependence of the climb velocity on the vacancy concentration X_v, we calculated $X_v D^v$ by using Eq. 3, where [following the work of Ammann *et al.* (*30*)] we put the attempt frequency equal to the Debye frequency ($\nu_D = 10^{13}$ Hz), the average jump distance ℓ equal to the nearest-neighbor distance in bridgmanite (ℓ = 2.5 Å) and ΔH^m equal to the migration enthalpy of Mg measured in bridgmanite at P = 24 GPa and T = 1973 to 2273 K (*31*).

To evaluate X_∞, we divided the simulation box in smaller boxes, as sketched in fig. S1. X_∞ is taken as the average vacancy concentration in the box j, where the dislocation is located, and in the first layer of the neighboring boxes (colored area in fig. S1). The displacements were calculated by using the explicit Euler forward algorithm, which is the standard integration method in DD, so that the dislocation position can be written as

$$\boldsymbol{x}_i(t + dt) = \boldsymbol{x}_i(t) + \boldsymbol{n}_i\, v_{c,i}\, dt \quad (7)$$

where dt is the simulation time step.

Update of the local and average vacancy concentration.

Each dislocation represents a source/sink of vacancies because it needs to emit or absorb vacancies to climb. Here, we considered the idea that each dislocation exchanges vacancies within the dislocations inside the same box. In particular, the rate of change of the local vacancy concentration in the box j is given by

$$\dot{X}_j = \frac{1}{L_{jx} L_{jy}} \sum_i^{N_j} v_{c,i} b \quad (8)$$

leading to

$$\Delta X_j = \frac{1}{L_{jx} L_{jy}} \sum_i^{N_j} v_{c,i} b\, dt \quad (9)$$

where the summation is performed over the N_j dislocations belonging to the box j; L_{jx} and L_{jy} are the linear dimensions of the box j. Similarly, the rate of change of the average vacancy concentration is given by

$$\dot{X} = \frac{1}{L_x L_y} \sum_i^N v_{c,i} b \quad (10)$$

and

$$\Delta \overline{X} = \frac{1}{L_x L_y} \sum_i^N v_{c,i} b \, dt \quad (11)$$

where N is the total number of dislocations and L_x and L_y are simulation box dimensions. We noticed that, because we defined the positive climb direction $\boldsymbol{n}_i$ as the direction of vacancy emission for the dislocation i, $v_{c,i}$ is positive when the dislocation emits vacancies. This resulted in an increase of average vacancy concentration $\overline{X}$ and on the jth box vacancy concentration X_j. On the contrary, when $v_{c,i}$ is negative, the dislocation absorbs vacancies leading to a decrease in $\overline{X}$ and X_j.

Plastic strain calculations.

Starting from the dislocation displacements $dx_i = v_{c,i}\, dt$, we can evaluate the contribution of climb to the plastic strain tensor ε. Each dislocation moving by climb during the time step dt produced an increment of the plastic strain: $d\beta_i = b\, dx_i/L_x L_y = b\, v_{c,i}\, dt/L_x L_y$, so that the climb plastic strain rate produced by the ith dislocation is $\dot{\beta} = b\, v_{c,i}\, dt/L_x L_y$. From the increment of the plastic strain, we can calculate climb contribution to the plastic strain rate and the increments of the plastic strain tensor ε per time step

$$d\varepsilon_{kl} = \sum_i^N \boldsymbol{Q}_i^{\alpha} d\, \beta_i = \sum_i^N \mathbf{b}_i \otimes \mathbf{b}_i\, d\, \beta_i = \frac{b}{L_x L_y} \sum_i^N \boldsymbol{b}_i \otimes \boldsymbol{b}_i\, v_{c,i} dt \quad (12)$$

In general, for each slip system, we can define the climb projection tensor ($\boldsymbol{Q}^{\alpha} = \boldsymbol{m}^{\alpha} \otimes \boldsymbol{m}^{\alpha}$), where $\boldsymbol{m}^{\alpha}$ is the slip direction for the slip system α. Because in our model we assumed that all the dislocations are edge in character, the slip direction $\boldsymbol{m}^{\alpha}$ for the slip system α coincides with the Burgers vector direction $\boldsymbol{b}^{\alpha}$.

Test for dislocation multiplication and annihilation.

DD simulations make use of local or constitutive rules to deal with dislocation reactions. Here, we included the possibility for dislocation with the same Burgers vector but opposite sign to annihilate when they are at a distance smaller than a critical radius $r_{annihil} = 20b$. This distance is much smaller than the linear box size $L = L_x = L_y$ that we considered in our simulations: $6 \times 10^3\, b < L < 2 \times 10^6\, b$. Additional rules were included in the 2.5D DD model to reproduce relevant 3D dislocation properties. In particular, a multiplication rule was used to reproduce the general 3D observation that the dislocation density ρ increases linearly with the plastic strain ε: $d\rho/d\varepsilon = m$. In analogy with the values adopted in previously published simulations, we imposed $m = 2 \times 10^{15}$ (*12*).

Diffusion creep: NH and Coble

In Fig. 4, strain rates corresponding to NH (*4*, *5*) and Coble creep (*6*) were calculated. Diffusion creep is the result of plastic strain produced by the motion of point defects. When a deviatoric stress is applied to a polycrystalline material, a heterogeneous stress state is built in the material. The vacancy concentration at grain boundaries under tension is larger than that at grain boundaries under compression, producing a flux of vacancies through the grains. This mechanism is referred to as NH creep. Under this loading condition (see sketch in Fig. 3A), the strain rate induced by migration of point defect through the bulk can be expressed by the following equation

$$\varepsilon_{NH} = \alpha \frac{D^{sd}}{d^2} \frac{\sigma\Omega}{k_B T} = \alpha \frac{X_v D^v}{d^2} \frac{\sigma\Omega}{k_B T} \quad (13)$$

NH creep takes into account mass transport through the bulk. Migration of point defects may also occur at grain boundaries. When migration at the interfaces between grains becomes the most effective diffusion path, the strain rate produced can be expressed by the following equation

$$\varepsilon_C = \alpha \frac{\delta D^{gb}}{d^2} \frac{\sigma\Omega}{k_B T} = \alpha \frac{\delta D^{v,gb} X_v}{d^3} \frac{\sigma\Omega}{k_B T} \quad (14)$$

This type of creep mechanism is referred to as Coble creep. In Eqs. 13 and 14, σ is the applied stress, Ω is the vacancy formation volume of bridgmanite, k_B is the Boltzmann constant, T is the temperature, α is a geometrical factor, here assumed to be equal to $^{16}/_3$ (*6*), and d is the average grain size. Diffusion strain rates reported in Fig. 4 were calculated by substituting $d = 0.1$ mm and $d = 10$ mm in Eq. 13 and Eq. 14, respectively. We notice that the grain size dependence of the strain rate is $1/d^3$ and $1/d^2$ for Coble and NH creep, respectively. Thus, Coble creep is expected to dominate at low grain size, but it is less favorable than NH creep at larger grain size.

The vacancy diffusion coefficient D^v used to calculate the NH creep rate (Eq. 13) was taken equal to the value used to calculate the climb velocity (Eq. 6). To compute the Coble creep strain rate, we wrote the grain boundary diffusion coefficient as $\delta D^{gb} = X_v \delta D^{v,gb} = X_v \delta \nu_a \ell^2 \exp\left(-\frac{\Delta H^{m,gb}}{k_B T}\right)$, where we consider $\nu_a = \nu_D = 10^{13}$ Hz and ℓ equal to the nearest-neighbor distance in bridgmanite $\ell = 2.5$ Å (as in Eq. 13), where $\Delta H^{m,gb} = 3.22$ eV is the migration enthalpy at the grain boundary measured in bridgmanite at $P = 25$ GPa and $T = 1673$ to 2073 K (*32*) and δ is the effective grain boundary thickness taken equal to 0.1 nm.

SUPPLEMENTARY MATERIALS

Supplementary material for this article is available at http://advances.sciencemag.org/cgi/content/full/3/3/e1601958/DC1

fig. S1. Sketch of the simulation box.

table S1. Parameters used to compute the glide mobility laws for dislocation in olivine, ringwoodite, and bridgmanite.

table S2. Parameters used to compute the climb mobility laws for dislocation in olivine, ringwoodite, and bridgmanite.

References (*33*, *34*)

REFERENCES AND NOTES

1. J. Hustoft, G. Amulele, J.-i. Ando, K. Otsuka, Z. Du, Z. Jing, S.-i. Karato, Plastic deformation experiments to high strain on mantle transition zone minerals wadsleyite and ringwoodite in the rotational Drickamer apparatus. *Earth Planet. Sci. Lett.* **361**, 7–15 (2013).
2. L. Miyagi, G. Amulele, K. Otsuka, Z. Du, R. Farla, S.-I. Karato, Plastic anisotropy and slip systems in ringwoodite deformed to high shear strain in the rotational Drickamer apparatus. *Phys. Earth Planet. Inter.* **228**, 244–253 (2014).

3. J. Girard, G. Amulele, R. Farla, A. Mohiuddin, S.-i. Karato, Shear deformation of bridgmanite and magnesiowüstite agregates at lower mantle conditions. *Science* **351**, 144–147 (2016).
4. F. R. N. Nabarro, Deformation of crystals by the motion of single ions, in *Report of a Conference on Strength of Solids* (Physical Society, 1948), pp. 75–90.
5. C. Herring, Diffusional viscosity of a polycrystalline solid. *J. Appl. Phys.* **21**, 437–445 (1950).
6. R. L. Coble, A model for boundary diffusion controlled creep in polycrystalline materials. *J. Appl. Phys.* **34**, 1679–1682 (1963).
7. A. Rozel, Impact of grain size on the convection of terrestrial planets. *Geochem. Geophys. Geosyst.* **13**, Q10020 (2012).
8. P. Glišović, A. M. Forte, M. W. Ammann, Variations in grain size and viscosity based on vacancy diffusion in minerals, seismic tomography, and geodynamically inferred mantle rheology. *Geophys. Res. Lett.* **42**, 6278–6286 (2015).
9. J. R. Weertman, Theory of steady-state creep based on dislocation climb. *J. Appl. Phys.* **26**, 1213–1217 (1955).
10. J. Weertman, Steady-state creep through dislocation climb. *J. Appl. Phys.* **28**, 362–364 (1957).
11. G. J. Weng, A micromechanical theory of high temperature creep. *J. Appl. Mech.* **54**, 822–827 (1987).
12. F. Boioli, P. Carrez, P. Cordier, B. Devincre, M. Marquille, Modeling the creep properties of olivine by 2.5-D dislocation dynamics simulations. *Phys. Rev. B* **92**, 014115 (2015).
13. J.-P. Poirier, Ed., *Creep of Crystals: High-temperature Deformation Processes in Metals, Ceramics and Minerals* (Cambridge Univ. Press, 1985).
14. H.-R. Wenk, P. Van Houtte, Texture and anisotropy. *Rep. Prog. Phys.* **67**, 1367–1428 (2004).
15. F. Boioli, A. Tommasi, P. Cordier, S. Demouchy, A. Mussi, Low steady-state stresses in the cold lithospheric mantle inferred from dislocation dynamics models of dislocation creep in olivine. *Earth Planet. Sci. Lett.* **432**, 232–242 (2015).
16. S. M. Keralavarma, T. Cagin, A. Arsenlis, A. Benzerga, Power-law creep from discrete dislocation dynamics. *Phys. Rev. Lett.* **109**, 265504 (2012).
17. W. B. Durham, C. Goetze, Plastic flow of oriented single crystals of olivine, 1: Mechanical data. *J. Geophys. Res.* **82**, 5737–5753 (1977).
18. S. Ritterbex, Ph. Carrez, P. Cordier, Modeling dislocation glide and lattice friction in Mg_2SiO_4 wadsleyite in conditions of the Earth's transition zone. *Am. Mineralogist* **101**, 2085–2094 (2016).
19. S. Ritterbex, P. Carrez, K. Gouriet, P. Cordier, Modeling dislocation glide in Mg2SiO4 ringwoodite: Towards rheology under transition zone conditions. *Phys. Earth Planet. Inter.* **248**, 20–29 (2015).
20. A. Kraych, P. Carrez, P. Cordier, On dislocation glide in $MgSiO_3$ bridgmanite at high-pressure and high-temperature. *Earth Planet. Sci. Lett.* **452**, 60–68 (2016).
21. F. Mompiou, L. Bresson, P. Cordier, D. Caillard, Dislocation climb and low-temperature plasticity of an Al–Pd–Mn quasicrystal. *Philos. Mag.* **83**, 3133–3157 (2003).
22. F. Mompiou, D. Caillard, Dislocation-climb plasticity: Modelling and comparison with the mechanical properties of icosahedral AlPdMn. *Acta Mater.* **56**, 2262–2271 (2008).
23. F. Mompiou, D. Caillard, Dislocations and mechanical properties of icosahedral quasicrystals. *C. R. Physique* **15**, 82–89 (2014).
24. F. R. N. Nabarro, Steady-state diffusional creep. *Philos. Mag.* **16**, 231–237 (1967).
25. G. Edelin, J. P. Poirier, Etude de la montée des dislocations au moyen d'expériences de flu age par diffusion dans le magnesium. I. Mécanismes de déformation. *Philos. Mag.* **28**, 1203–1210 (1973).
26. G. Edelin, J. P. Poirier, Etude de la montée des dislocations au moyen d'expériences de fluage par diffusion dans le magnesium. II. Mesure de la vitesse de montée. *Philos. Mag.* **28**, 1211–1223 (1973).
27. R. Le Hazif, G. Edelin, J. M. Dupouy, Diffusion creep by dislocation climb in beryllium and Be-Cu single crystals. *Metall. Trans.* **4**, 1275–1281 (1973).
28. J. Durinck, B. Devincre, L. Kubin, P. Cordier, Modeling the plastic deformation of olivine by dislocation dynamics simulations. *Am. Mineralogist* **92**, 1346–1357 (2007).
29. D. Caillard, J. L. Martin, Eds., *Thermally Activated Mechanisms in Crystal Plasticity* (Pergamon, 2003).
30. M. W. Ammann, J. P. Brodholt, D. P. Dobson, Simulating diffusion. *Rev. Mineral. Geochem.* **71**, 201–224 (2010).
31. C. Holtzapfel, D. C. Rubie, D. J. Frost, F. Langenhorst, Fe-Mg interdiffusion in $(Mg,Fe)SiO_3$ perovskite and lower mantle reequilibration. *Science* **309**, 1707–1710 (2005).
32. A. Shimojuku, T. Kubo, E. Ohtani, T. Nakamura, R. Okazaki, R. Dohmen, S. Chakraborty, Si and O diffusion in $(Mg,Fe)_2SiO_4$ wadsleyite and ringwoodite and its implications for the rheology of the mantle transition zone. *Earth Planet. Sci. Lett.* **284**, 103–112 (2009).
33. D. Yamazaki, T. Kato, H. Yurimoto, E. Ohtani, M. Toriumi, Silicon self-diffusion in $MgSiO_3$ perovskite at 25 GPa. *Phys. Earth Planet. Inter.* **119**, 299–309 (2000).
34. H. Fei, C. Hegoda, D. Yamazaki, M. Weidenbeck, H. Yurimoto, S. Shcheka, T. Katsura, High silicon self-diffusion coefficient in dry forsterite. *Earth Planet. Sci. Lett.* **345**, 95–103 (2012).

Acknowledgments

Funding: We acknowledge financial support from the European Research Council under the Seventh Framework Programme (FP7 ERC grant no. 290424–RheoMan). **Author contributions:** The author list is set in alphabetic order. P. Cordier designed the study and supervised it with P. Carrez. F.B. modelled the creep with B.D. S.R. performed calculations on ringwoodite with K.G. and P. Carrez. A.K. modelled the dislocation glide in bridgmanite with P. Carrez and P.H. P. Cordier wrote the paper with feedback and contributions from all co-authors. All authors discussed and interpreted the results. **Competing interests:** The authors declare that they have no competing interests. **Data and materials availability:** All data needed to evaluate the conclusions in the paper are present in the paper and/or the Supplementary Materials. Additional data related to this paper may be requested from the authors.

Submitted 18 August 2016
Accepted 2 February 2017
Published 10 March 2017
10.1126/sciadv.1601958

Citation: F. Boioli, P. Carrez, P. Cordier, B. Devincre, K. Gouriet, P. Hirel, A. Kraych, S. Ritterbex, Pure climb creep mechanism drives flow in Earth's lower mantle. *Sci. Adv.* **3**, e1601958 (2017).